Bioceramic powders for bone regeneration modified by high-pressure CO2 process

Clémentine Aubry, Séverine Camy, Christèle Combes, Olivier Marsan, Thibault Canceill, Sophie Cazalbou

Bioceramic powders for bone regeneration modified by high-pressure CO_2 process

C. Aubry[1,2], S. Camy[2], C. Combes[3], O. Marsan[3], T. Canceill[1], and S. Cazalbou[1,*]

[1] CIRIMAT, CNRS, Université de Toulouse, Université Toulouse 3 - Paul Sabatier, Toulouse, France
[2] Laboratoire de Génie Chimique, CNRS, INPT, UPS, Université de Toulouse, Toulouse, France
[3] CIRIMAT, CNRS, INPT-ENSIACET, Université de Toulouse, Toulouse, France

ABSTRACT

Non-stoichiometric nanocrystalline apatites present enhanced bioactivity compared to stoichiometric hydroxyapatite. The purpose of this work was to modify the calcium phosphates (CaP) generally used to prepare bioactive ceramics in the aim of obtaining a biomimetic apatite powder. Hydroxyapatite (HA) powder, amorphous tricalcium phosphate (amTCP) powder and a blend of these two were modified by means of an innovative, simple, "green" carbonation process, involving water and high-pressure CO_2 (80 bar). This process induced a modification of the CaP, which is sensitive to the environment in which it is located and, in particular, to the pH variations that occur during the treatment phase (decrease in the pH) and during the degassing phase (return to neutral pH). FTIR and Raman spectroscopy, XRD and SEM analyses showed that, depending on the type of initial CaP powder, high-pressure CO_2 treatment led to the formation of different types of calcium phosphate phases. This process allowed partial dissolution of the initial powder, mainly of TCP when present, and precipitation of a new CaP phase. HA and HA/amTCP powders were transformed into a mixture of OCP and immature carbonated apatite (PCCA) phases, including OCP maturation/transformation into PCCA. In the case of amTCP powder, a DCPD phase was also present due to the high TCP solubility and an earlier precipitation during the degassing step. This work shows the great potential of such an innovative low-temperature and high-pressure process to transform HA, HA/TCP and TCP powder into bioactive biphasic ceramics composed of OCP and PCCA similar to bone mineral.

Address correspondence to E-mail: sophie.cazalbou@univ-tlse3.fr
https://doi.org/10.1007/s10853-020-04476-y

Introduction

The complex chemistry and structure of bone mineral have been widely investigated in the recent decades. It has been shown to be composed of a calcium-deficient carbonated apatite (PCCA) of chemical formula $Ca_{8.3}\ \square_{1.7}\ (PO_4)_{4.3}\ (HPO_4)_{0.7}\ (CO_3)_{1.0}\ (CO_3.OH)_{0.3}\ \square_{1.7}$ [1]. Its lacunar structure and the presence of a hydrated layer make it very reactive and therefore suitable for bone regeneration [2]. Studies concerning bone mineralization have shown the presence of CO_3^{2-} or HPO_4^{-} ionic groups in the nanocrystalline apatite of newly formed bone [3]. These newly formed apatite nanocrystals also present a hydrated layer on their surface, which has been shown to become thinner with time and maturation [2, 4–6]. This hydrated layer includes mainly labile non-apatitic bivalent ions and is responsible for the surface properties (ion exchange, adsorption properties, etc.) of biological apatites and their synthetic analogues. The reactivity of the mineral phase, initially high in the immature stage, decreases as the mineral ages.

Biomimetic apatite, a calcium phosphate very similar to bone mineral, can be considered as one of the main candidates for use in materials designed for bone regeneration. However, although it has been widely studied in the literature [5, 7, 8], its development is limited to date because its production is difficult to industrialize. The preparation of such biomimetic apatite requires a low-temperature and an aqueous synthesis process. The proportion of calcium and phosphate ions in the solution and the pH are critical parameters [2, 9] .

Stoichiometric hydroxyapatite (HA, $Ca_{10}(PO_4)_6(OH)_2$) is the most developed and commercialized of the various calcium phosphates available because of its similarity with bone apatite in terms of chemical composition and crystalline structure. Tricalcium phosphates (TCP, $Ca_3(PO)_4$) are also involved in bone substitute materials, in the form of dense or porous ceramics, coatings on metallic prostheses, cements and composites. Whatever the type of TCP phase (amorphous, α or β), TCP is considered as more soluble than stoichiometric HA in most environments [9]. HA and β-TCP are often associated in the preparation of the well-known biphasic calcium phosphate (BCP) ceramics. Most macroporous sintered BCP ceramics are made of HA/β-TCP with mass ratios varying from 60/40 to 80/20 [10]. These porous bioceramics are processed by gel casting or replication of polymer sponge, depending on the target porosity and final mechanical strength, and then sintered at high temperature [11]. The use of high temperatures leads to HA/β-TCP ceramic scaffolds with poor reactivity. Activating this kind of medical device by converting at least the surface into a biomimetic apatite phase could be an interesting way to enhance the bioactivity of such bioceramics. This is the idea developed by Autefage [12] in their work related to the coating of porous HA/β-TCP scaffolds with nanocrystalline apatite. In this approach, the surface of well-known macroporous BCP bioceramics is modified in order to obtain a phase with enhanced biomimetic properties, improved physico-chemical and biological properties—especially protein adsorption ability, and osteoinduction properties. As mentioned earlier, obtaining such a biomimetic apatite requires an aqueous environment and a low temperature.

Supercritical CO_2, i.e. CO_2 above its critical temperature (31 °C) and pressure (74 bar), has been used recently as a solvent for shaping or doping in the field of biomaterials [13–17]. It has the main advantages of low process temperature and leaving the material totally free of solvent at the end of the process, since CO_2 returns to its gaseous state after depressurization [18–20]. Interestingly, when in contact with water, CO_2 dissolves to form carbonic acid, thus inducing a pH modification of the water (acidification), a key parameter that controls the solubility of CaP phases. This leads to the possibility of precipitation of new phases that are likely to integrate carbonate ionic species present in the aqueous environment.

The solubility of CO_2 in water, and thus the pH of the aqueous solution, is dependent on pressure and temperature, which can be adjusted to material requirements [21]. This ability has been used in bone regeneration to coat some bone substitute materials or prostheses with an apatite layer [22]. A calcium phosphate supersaturated solution was used, and the pH was decreased by CO_2 bubbling in order to avoid the precipitation of CaP at the first stage. Bubbling was then stopped, causing the pH to rise again and the apatite to precipitate [22].

In its gaseous state, CO_2 has also been used to allow HA carbonation. At high temperature (800 °C) and with a constant flux of CO_2, it has been shown that some of the hydroxide ions can be replaced by

carbonate ions (Type A carbonate) in the HA structure [9].

To conclude, gaseous or supercritical CO_2 has been used in the field of biomaterials as a carbonating agent and a pH modifier. In the work presented here, CO_2 at high pressure and low temperature, in contact with water as the liquid phase, is used to modify calcium phosphate powders of biological interest in order to design bioactive bone substitute materials. The objective of this work was to demonstrate that the process can allow reactive and carbonated calcium phosphate materials to be obtained that are similar to bone mineral and should enhance bioactivity. The clean, reversible process of CO_2 treatment was implemented to partially solubilize several calcium phosphate phases [non-thermally treated HA, amTCP and a blend of both these powders 65:35 (*w*/*w*)] and simultaneously induce a precipitation of ionic species (Ca^{2+}, PO_4^{3-}, etc.) in situ, leading to a new ceramic phase.

Materials and methods

Experimental set-up

The calcium phosphate phases used in this study are conventionally employed as starting powders in the manufacture of biphasic (HA/TCP) porous sintered ceramics.

Non-thermally treated hydroxyapatite (HA) powder was provided by Teknimed (Blocky®, France). Amorphous TCP (amTCP) powder was synthesized by co-precipitation using a method developed by Heughebaert [23]. As a first step, the selected powder was put into water (separately or as a blend of HA/amTCP with a mass ratio of 65:35). It was then treated with the high-pressure CO_2 process.

A supercritical cell (E3100) from Quorum Technologies, UK, was used to perform high-pressure CO_2/water treatment. The cell temperature was regulated by a thermostated bath (Isotemp Fisher Scientific, USA).

XRD and FTIR spectroscopy analyses were performed before and after treatment.

Experimental procedure

Finely ground (0.1 g) HA or amTCP powder or a blend of both these powders 65:35 (*w*/*w*) was placed in a beaker, covered with deionized water at a liquid-to-solid mass ratio of 2 (L/S = 2) and introduced into the supercritical CO_2 cell initially regulated at 5 °C. The device was then filled with liquid CO_2, before being heated to 37 °C (Fig. 2 part 1). As the temperature rose, the pressure increased to reach a final pressure of 80 bar. The CO_2 dissolved in the water, and carbonic acid was formed according to Eqs. 1–3. This led to the acidification of the solution at a theoretical pH of 3.2 under these temperature and pressure conditions [21], the CO_2 solubility being dependent on temperature and pressure.

$$CO_2 + H_2O \rightarrow H_2CO_3 \quad (1)$$

$$H_2CO_3 + H_2O \rightarrow HCO_3^- + H_3O^+ \quad (2)$$

$$HCO_3^- + H_2O \rightarrow CO_3^{2-} + H_3O^+. \quad (3)$$

The system was maintained at 37 °C and 80 bar for 4 h (Fig. 1 part 2) and then slowly depressurized over 30 min (Fig. 1 part 3). A low temperature was chosen to respect the biomimetic apatite formation requirements. Such a temperature favours low pH as shown in the literature [21]. The decrease in the pressure and the progressive degassing of dissolved CO_2 induced a gradual increase in pH until neutrality was again attained. At the end of the experiment, some of the powder remained at the bottom of the beaker and is referred to as *Bottom Powder* in the study. The entire beaker containing the *Bottom powder* and the aqueous environment was then placed in a ventilated oven at 50 °C for 1 h to accelerate the water evaporation (Fig. 1 part 4). During this step, a new deposit formed at the air–water interface and this new solid phase is referred to as *Top Powder*. It slowly nucleated at the surface of the water phase to finally cover the entire surface of the solution. This solid film of *Top Powder* was then recovered and dried in a ventilated oven for 24 h at 50 °C at the same time as the *Bottom Powder* (Fig. 1 part 5).

It is important to highlight the impossibility of following the pH value and the calcium and phosphate concentrations directly at each step of the process, due to the pressure level during the process. So, only the final powders were analysed, by the complementary characterization techniques described below.

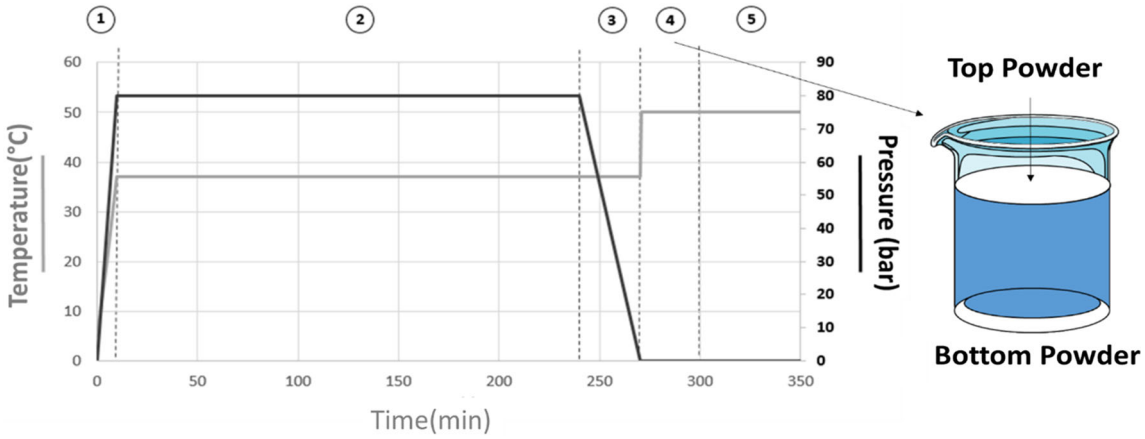

Figure 1 Parameters (temperature and pressure) set during the processing steps (1—pressurization, 2—treatment for 4 h, 3—depressurization, 4—precipitation of a new phase at the surface, 5—beginning of the 24-h drying step).

Morphological characterization

Morphological characterization of powders (*Bottom Powders* and *Top Powders)* was carried out by SEM using an SEM-FEG JSM 7100F TTLS (Field Emission Gun, JEOL, Japan). Powders were immobilized by conductive carbon adhesive tape on aluminium stubs and coated with gold (SI50B sputter coater, Edwards, UK) for 90 s.

Structural and chemical analyses

The crystalline phases constituting the calcium phosphate powders before and after CO_2 treatment were identified using X-ray diffraction (XRD, Bruker AXS GmbH, Karlsruhe, Germany) with Cu Kα radiation (λ = 1.5406 Å) from 0° to 80° (2θ). Then, the diffraction data were processed with Match! 1.11 software.

Fourier-transform infrared spectroscopy (FTIR) analysis using the transmission mode with the KBr pellet method was performed to determine the chemical composition of the powders at the molecular level. This technique identifies the presence of different ionic groups and bonds such as carbonate and phosphate and their presence or absence in a hydrated layer environment, i.e. in apatitic or non-apatitic hydrated environments. The FTIR spectra were collected using a PerkinElmer 1700 spectrometer (USA) in the range 4000–400 cm^{-1} at a resolution of 2 cm^{-1}. OMNIC 9.6.251 software was used to process the data.

Spectral decompositions were carried out using the LabSpec 6 software after subtraction of a linear baseline in the 700–450 cm^{-1} domain corresponding to the υ_2 υ_4 (PO_4) and υ_L (OH) vibration modes of phosphate and hydroxide ions. The positioning of each contributing band existing in this spectral domain was based on the reported data [4, 24]: at 470 cm^{-1} corresponding to υ_2 (PO_4^{3-}), 534–530 cm^{-1} (non-apatitic HPO_4^{2-}), 550 cm^{-1} (apatitic HPO_4^{2-}), 601/575/560 cm^{-1} (apatitic PO_4^{3-}), 617 cm^{-1} (non-apatitic PO_4^{3-}), 631 cm^{-1} (υ_L (OH^-)), 670 cm^{-1} (H_2O libration mode) and the specific bands of the OCP phase at 627 cm^{-1}, 524 cm^{-1} (υ_4 PO_4) and 466 cm^{-1} (υ_2 PO_4). The bands were considered as Gaussian and/or Lorentzian in shape.

In order to determine the distribution of the previously identified CaP phases in the *Top Powder*, Raman spectroscopy was also performed. Powders were analysed using a LabRAM HR 800 confocal microscope (Horiba Jobin Yvon, Japan). The results were analysed and decomposed with LabSpec 6 software. Spectral decompositions were carried out, after subtraction of a linear baseline, in the 1200–800 cm^{-1} domain corresponding to the υ_3 (PO_4). The positioning of each contributing band existing in this spectral domain was based on previously reported data [4], the main bands being at 961 cm^{-1} (υ_1 PO_4) for the apatitic structure and 966, 958 cm^{-1} (υ_1 PO_4) for OCP. The bands were considered as Gaussian and/or Lorentzian in shape. This technique allowed us to observe the sample (x and y axes) and focus on a specific part of the sample. Furthermore, a mapping on the z axis allowed 3D investigation on the samples. A 3D mapping of part of the HA/amTCP *Top Powder* plate was obtained, and three

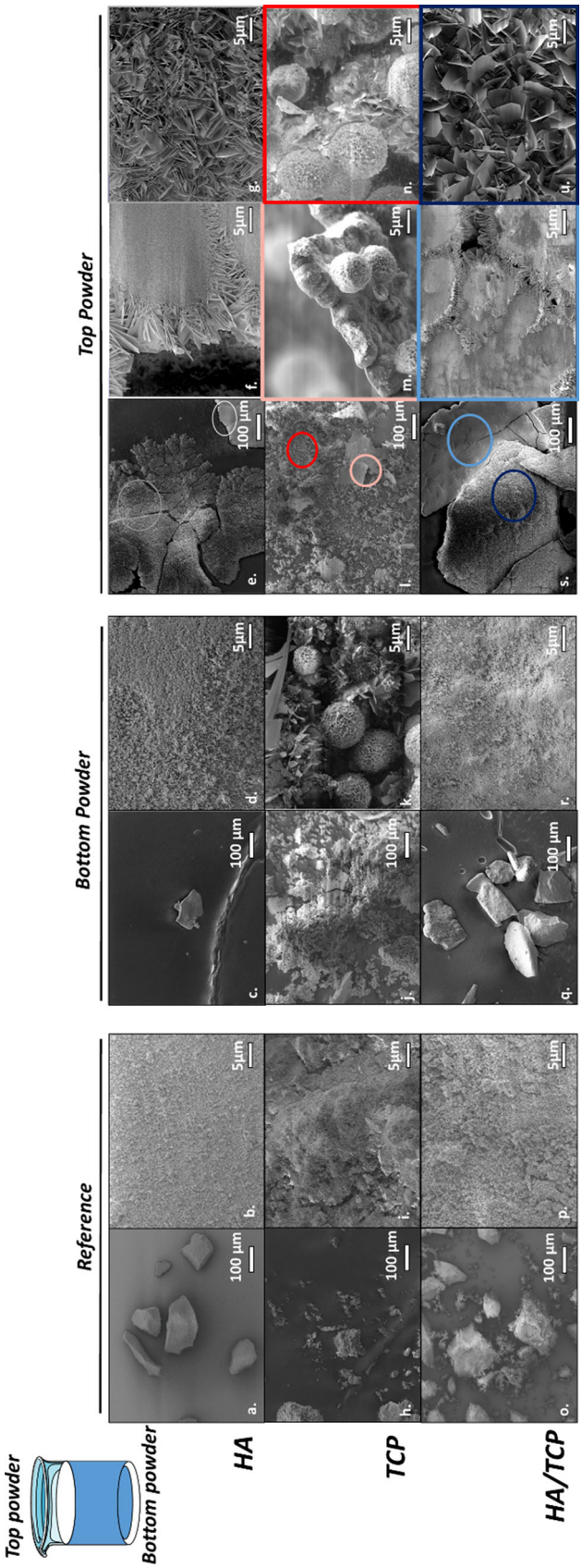

Figure 2 SEM micrographs of the HA, amTCP and HA/amTCP reference powders and their corresponding Bottom and Top Powders after high-pressure CO_2 treatment.

different z values were chosen: z = 0, 5 and 10 µm, to analyse the upper, middle and lower surfaces (0–5–10 µm) of the plate.

Results and discussion

Morphological study

SEM observations were made on the reference samples and high-pressure CO_2-treated powders (*Bottom Powder* and *Top Powder*) (Fig. 2). Each line of the figure corresponds to a specific sample (HA, amTCP or HA/amTCP mixture).

The HA reference micrograph shows particles with a smooth surface in the 150–200 µm range (Fig. 2a). As shown in Fig. 7c, d, the *Bottom Powder* obtained after the treatment presented a very similar surface aspect. In contrast, the *Top Powder* phase presented no trace of the original HA grains but a complex plate-like structure (Fig. 2e). This plate was composed of a flat surface (Fig. 2f) on the side corresponding to the atmosphere–water interface, and a surface covered with entangled sheet-like crystals 5 µm in width (Fig. 2g) on the other side, facing the water bulk. This sheet-like morphology is typical of OCP crystals [9]. This side of the plate seemed to be composed of small plates merged into a big one covering the whole surface.

When compared to the HA reference, the amTCP reference SEM image shows smaller (20–30 µm) grains with a relatively smooth surface (Fig. 2h), whereas the corresponding *Bottom* and *Top Powders* appear to be very different. The remaining *Bottom Powder* presents several kinds of spherical structures with a smooth or "flower-like" [25] surface, covered with sheets (Fig. 2k). Calcium carbonate, hydroxyapatite or OCP have shown the ability to form such structures when subjected to different processes including CO_2 templating in aqueous systems [26–28]. Some rare "ribbon-like" structures can also be observed (Fig. 2k) and could indicate the presence of DCPD [9]. Unlike the HA *Top Powder*, the amTCP *Top Powder* is made of a complex plate-like structure. The side of the main plate oriented towards the

atmosphere/water interface is flat. The opposite side, facing the water bulk, shows several spherical structures with flat or "flower-like" surfaces, as in *Bottom Powder*, that are mainly organized in large plates (Fig. 2m, n). This complex plate structure also seems to be composed of merged smaller ones.

As expected, the HA/amTCP reference was a mixture of HA and amTCP reference morphologies, with a very smooth surface for both types of grains (Fig. 2o). The HA/amTCP *Bottom Powder* was composed of large grains with no small grains (Fig. 2q). This observation would confirm the dissolution of a part of the initial powder in the acidic environment induced by the dissolution of CO_2 in water. The HA/amTCP *Top Powder* (Fig. 2s) was similar to the raw HA one (Fig. 2e). A main plate (Fig. 2s) with one flat (Fig. 2t) and one sheet-like face (Fig. 2u) was composed of smaller plates that had merged together. The sheet-like crystals on the totally immerged side (Fig. 2u) were larger than those observed on the HA *Top Powder* (Fig. 2g). They showed the characteristic morphology of OCP crystals (Fig. 2c).

Whatever the original powder, the CO_2 treatment led to a morphological modification of the powder used.

Both materials, HA and HA/amTCP, behaved similarly during the treatment. In both cases, the *Bottom Powder* remained unchanged, while the *Top Powder* formed a large plate, flat on one side and covered with entangled platelets on the other. The only observable difference between samples lay in the size of these platelets, which were larger in the case of HA/amTCP *Top Powder*.

In contrast, observations made in the case of amTCP showed different tendencies. After the high-pressure CO_2 treatment, the original powder was no longer visible but unique spherical structures, flat or covered with platelets, and therefore called "flower-like", could be observed on both *Bottom* and *Top Powders*. Unlike in the case of HA and HA/amTCP powders, the *Top Powder* was organized in a complex plate-like structure and was flat at the atmosphere/water interface.

Structural and chemical analyses

X-ray diffraction (XRD)

XRD characterization was performed in order to identify the crystalline phases present in each type of powder (HA, amTCP, HA/amTCP), before and after the treatment. The results are presented in Fig. 3. It should be noted that small available amounts of *Top Powder* and amTCP *Bottom Powder* might be the reason for a slightly blurred signal. In addition, the halos present at around 8° and 14° on these X-ray diffractograms might be due to artefacts from the sample holder.

As expected, the X-ray diffraction pattern of HA reference in Fig. 3a corresponds to a well-crystallized hydroxyapatite (JCPDS 00-009-0432). After CO_2 treatment, no modification of the HA powder was observed as all the diffraction peaks of the HA *Bottom Powder* diffractogram were assigned to HA. However, the HA *Top Powder* corresponds to a mixture of a poorly crystalline apatite and octacalcium phosphate (OCP) (JCPDS 00-026-1056), which is in agreement with the characteristic structures observed on SEM images.

Figure 3b presents X-ray diffractograms corresponding to experiments with amTCP powder. It can be observed that the X-ray pattern of the amTCP reference powder also corresponds to what was expected, i.e. an amorphous TCP. However, the amTCP *Bottom Powder* and *Top Powder* X-ray diffraction diagrams differ significantly from that of the initial raw powder and correspond to a mixture of OCP, apatite and dicalcium phosphate dihydrate (DCPD) (JCPDS 00-011-0293). The presence of DCPD could be consistent with the observation of ribbon-like structures.

The HA/amTCP X-ray diffractogram of reference powder presented in Fig. 3c shows only the diffraction peaks of HA. The amorphous phase is barely visible with XRD analysis, and amTCP is not the main phase in the HA/amTCP mixture (35% w/w of amTCP). Similarly to the case of HA samples, the HA/amTCP *Bottom Powder* only corresponds to HA. However, in the case of the *Top Powder*, OCP and poorly crystalline apatite phases can be identified.

The XRD analysis shows that, in accordance with SEM observation, several similarities due to high-pressure CO_2 treatment can be detected between HA and HA/amTCP evolution. XRD diagrams of *Top* and *Bottom Powders* shown in Fig. 3a, c are very similar and correspond to a mixture of poorly crystalline apatite and OCP. However, in the case of amTCP (Fig. 3b), the original phase is no longer visible in the corresponding *Bottom Powder*. The amTCP *Bottom* and *Top Powders* show the same phases as HA

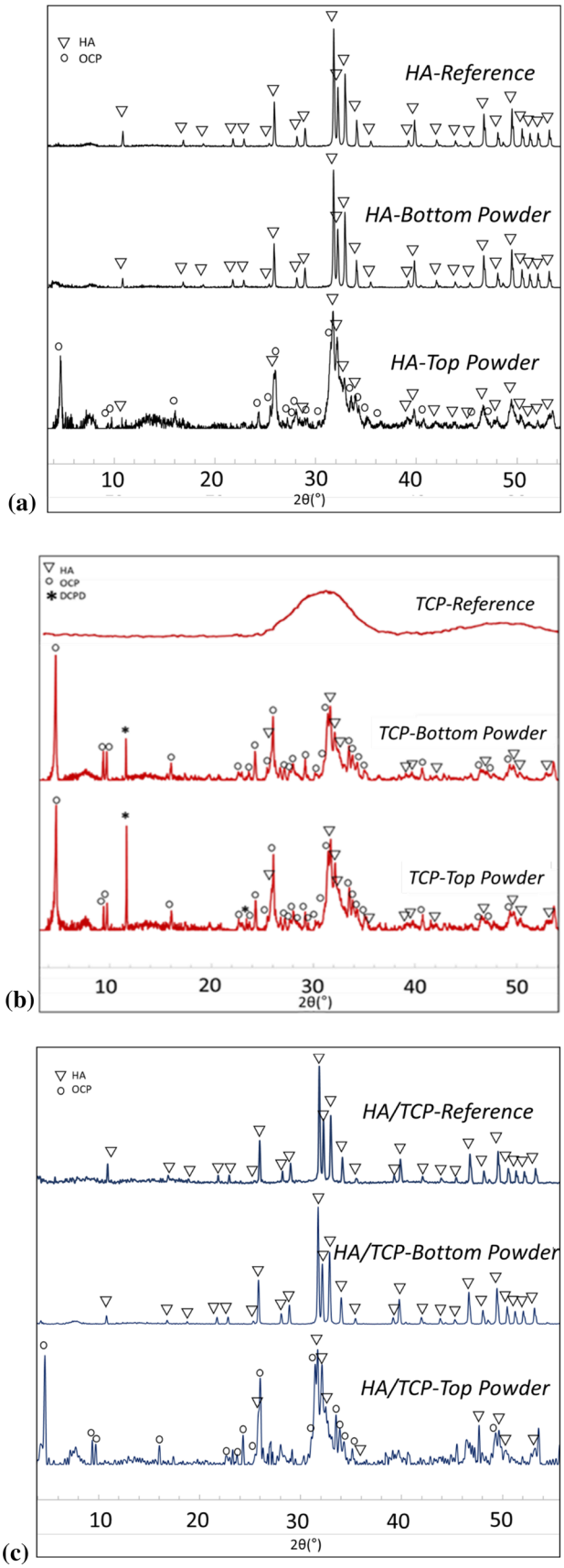

◀**Figure 3** XRD pattern of **a** HA powder: reference, Bottom Powder, Top Powder; **b** amTCP powder: reference, Bottom Powder, Top Powder; **c** HA/amTCP powder: reference, Bottom Powder, Top Powder.

and HA/amTCP *Top powder*, i.e. they show the presence not only of apatite and OCP phases, but also of an additional DCPD phase.

Fourier-transform infrared (FTIR) spectroscopy

The FTIR spectroscopic analysis performed on HA, amTCP, HA/amTCP reference and treated powders (*Bottom* and *Top Powders*) identified some of the anionic groups present in the different crystalline phases that were characterized by XRD. In particular, FTIR spectroscopy distinguished the presence of phosphate and carbonate groups present in apatitic and labile non-apatitic environments (in the hydrated layer at the surface of apatite nanocrystals). Non-apatitic PO_4^{3-} and HPO_4^{2-} groups were identified by the presence of bands at 617 and 530 cm^{-1} [26], and the presence of apatitic and labile non-apatitic carbonate groups was evidenced in the 1600–1300 cm^{-1} and also in the 900–800 cm^{-1} domains. The presence of the OH band (3175 cm^{-1}) [4] also helped to follow partial or complete modifications undergone by the original stoichiometric hydroxyapatite phase.

As observed on the FTIR spectra presented in Fig. 4 for HA samples, the HA *Bottom Powder* presented the same bands as the non-treated HA powder [962 cm^{-1} (υ_1 PO_4), 601 cm^{-1}, 575 cm^{-1}, 561 cm^{-1} (υ_4 PO_4) and 3175 cm^{-1} (OH)], the carbonate band, visible in the 1600–1400 cm^{-1} domain, being slightly more intense in the case of HA *Bottom Powder* [4]. This increase was even more pronounced in the case of HA *Top Powder*. More specifically, different types of carbonates, mainly type B and a labile one [1540 cm^{-1} (type A), 1500 cm^{-1} (labile), 1460–1470 cm^{-1} (type A and B), 1420 cm^{-1} (type B and labile)], could be observed after the CO_2 treatment [4]. Knowing that HA *Top Powder* is composed of OCP and apatite and that carbonated OCP does not exist, the carbonate species were necessarily integrated in the apatite structure detected by XRD. The identification of labile carbonates testifies to the presence of a hydrated layer on the apatite crystals of the *Top Powder*. These results demonstrate that the apatite formed after high-

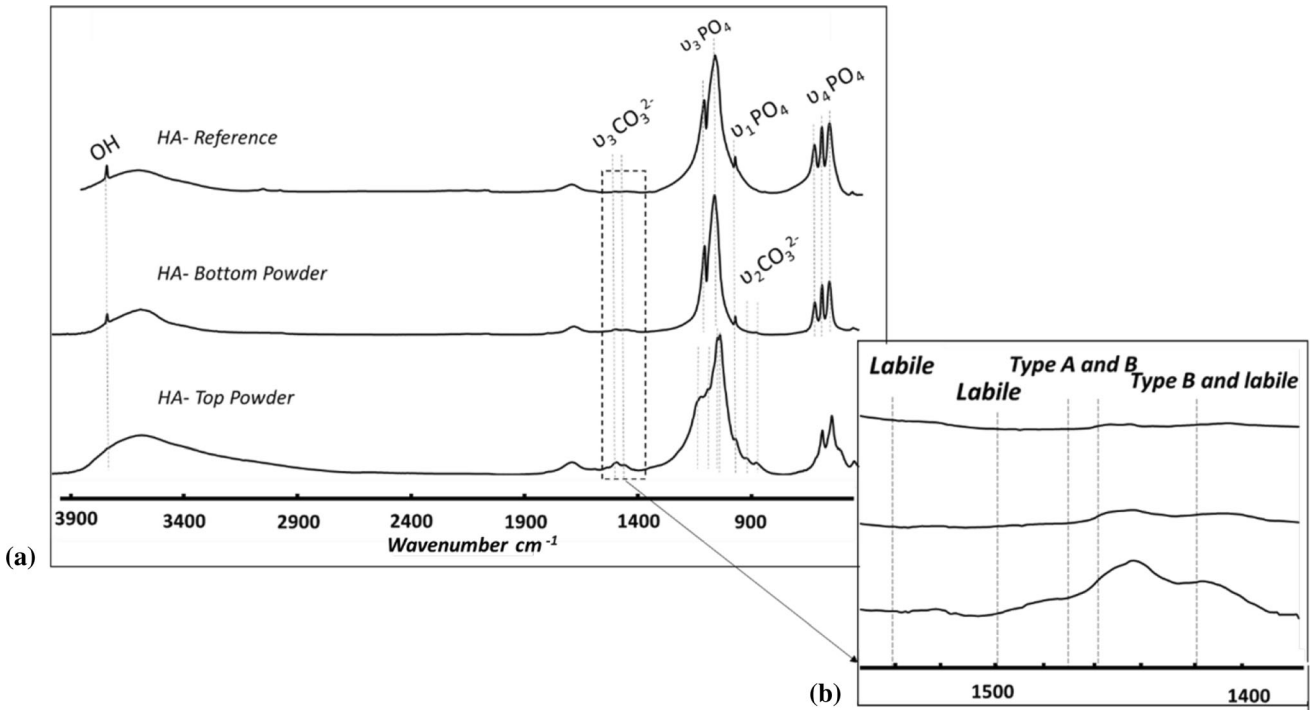

Figure 4 FTIR spectra of HA reference powder, Bottom Powder, Top Powder, **a** 4000–400 cm^{-1} domain and **b** 1580–1380 cm^{-1} domain.

pressure CO_2 treatment applied to HA powder corresponds to a poorly crystalline carbonated apatite (PCCA). In addition, some characteristic bands of OCP phase are also observed (1300–1000 cm^{-1} (υ_3 PO_4); 962 cm^{-1} (υ_1 PO_4); 917 cm^{-1} and 861 cm^{-1} (P–OH of HPO_4^{2-}); 627 cm^{-1}, 601 cm^{-1}, 575 cm^{-1}, 560 cm^{-1} and 524 cm^{-1} (υ_4 PO_4); etc.) [4]. Finally, it can be concluded from the XRD and FTIR spectroscopic data that the HA *Bottom Powder* corresponds to initial HA with a small amount of PCCA, whereas the *Top Powder* is made up of a mixture of OCP and PCCA with different kinds of carbonates including labile carbonates.

The FTIR spectra of amTCP samples (Fig. 5) reveal significant differences between the reference sample and treated powders. The FTIR spectra of both *Bottom* and *Top Powders* show characteristic bands of OCP phase [27], confirming the XRD results. An increase in the intensity of carbonate bands (A, B and labile types) can be observed on the *Bottom Powder* spectrum and is even more pronounced on that of the *Top Powder*. The increase in carbonates from the *Bottom* to the *Top powder* was also observed in the case of treated HA powders.

It can be observed that the HA/amTCP reference spectrum is closer to that of the HA than to that of the amTCP (Fig. 6) and does not result from a simple addition of HA and amTCP bands. However, a broadening of the phosphate group bands corresponding to HA can be observed, due to the amTCP phosphate band contribution. The HA/amTCP *Bottom Powder* spectrum is typical of that of HA, in agreement with the XRD results (Fig. 3c). Nonetheless, the FTIR analyses allow different types of carbonate species to be identified, mainly B and labile, which are present in small amounts. The HA/amTCP *Top Powder* spectrum shows bands characteristic of OCP and apatite, as expected from XRD analysis, with an increase in the bands corresponding to the different types of carbonate (A, B and labile). The evolution of carbonate bands (1600–1330 cm^{-1}) between the reference, *Bottom* and *Top* powder spectra is very similar to what was observed for pure HA and amTCP powders, as described previously. This increase could be confirmed by evaluating the area under the peaks between 1600 and 1300 cm^{-1}.- The measurement was made on the spectrum normalized on the υ_3 PO_4 groups. An average increase of 55% was observed between the *Bottom* and *Top powder* spectra for each experiment. Finally, the XRD and FTIR spectroscopy data seem to indicate considerable similarity between HA and HA/amTCP behaviour.

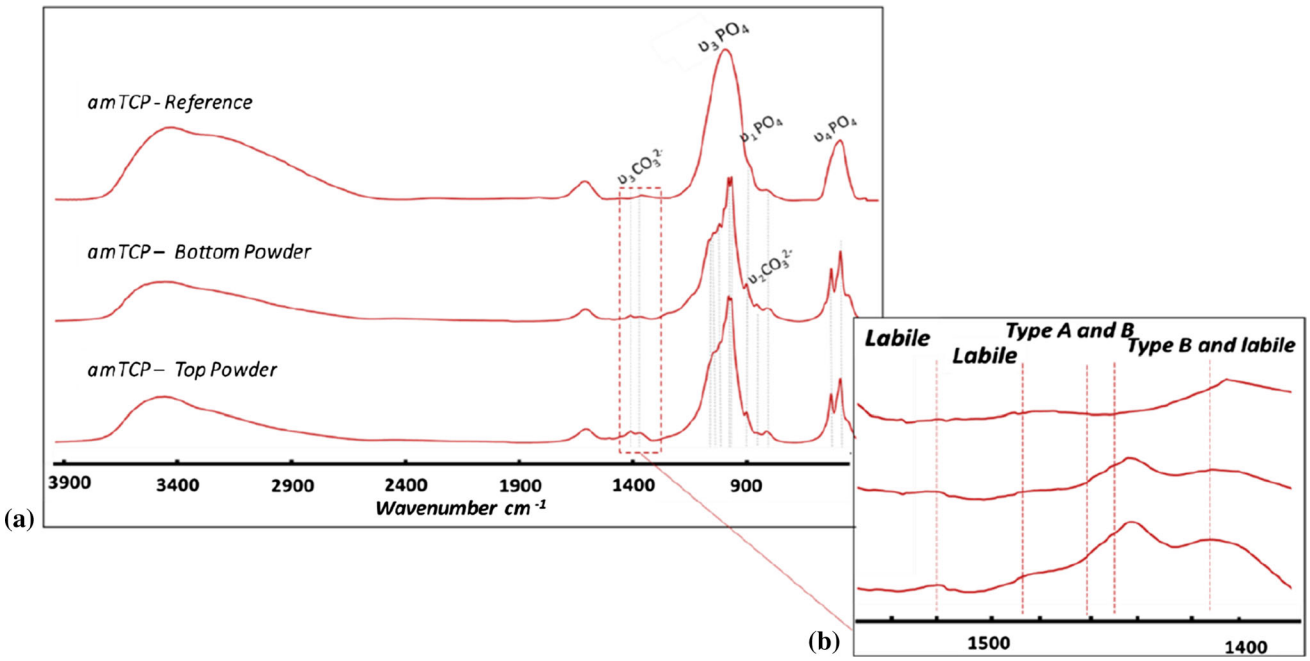

Figure 5 FTIR spectra of amTCP reference powder, Bottom Powder, Top Powder: **a** 4000–400 cm^{-1} domain and **b** 1580–1380 cm^{-1} domain.

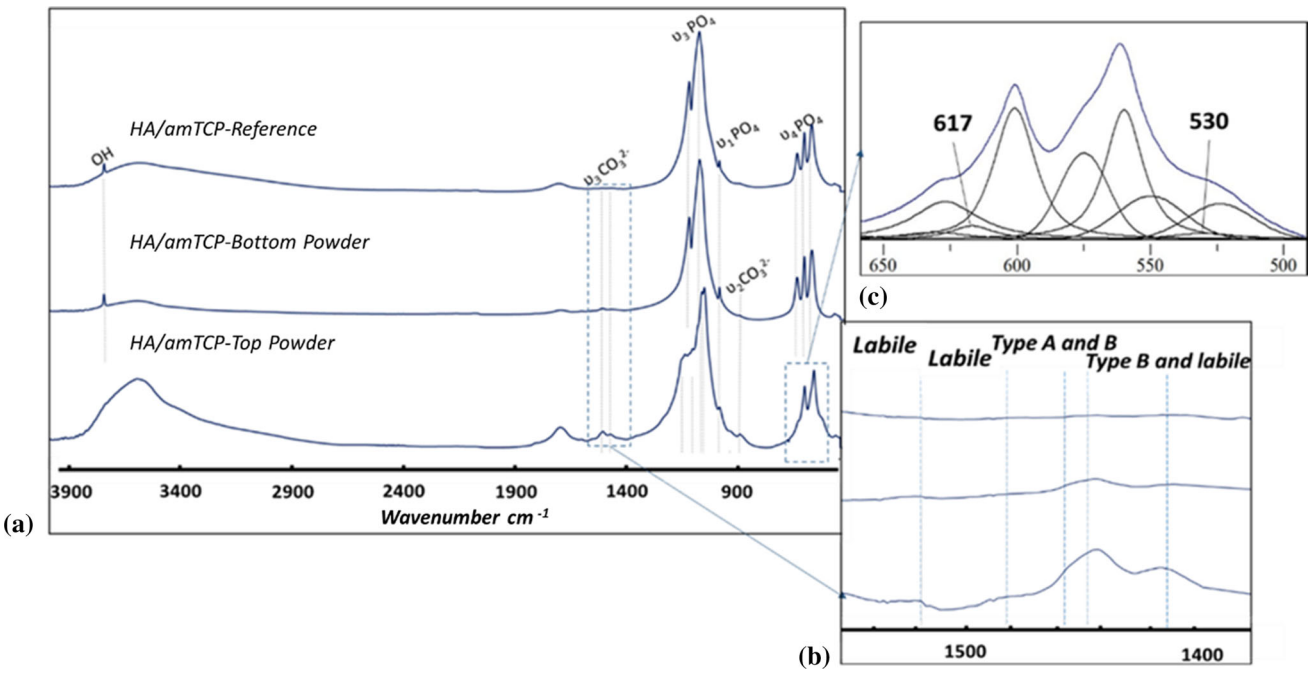

Figure 6 FTIR spectra: HA/amTCP reference powder, Bottom Powder, Top Powder: **a** 3900–400 cm^{-1} domain, **b** 1580–1380 cm^{-1} domain and **c** example of band decomposition in the 700–450 cm^{-1} domain.

To conclude, the FTIR analyses tend to demonstrate that, during the high-pressure CO_2 process, a carbonation phenomenon occurs whatever the calcium phosphate powders considered. For all phases (HA, amTCP and HA/amTCP), the bands corresponding to carbonate ions are present on the spectra of *Bottom Powder* and *Top Powder* samples. From a global point of view, the *Bottom Powder* samples seem

to be less carbonated than the *Top Powder* ones. Considering that, according to the literature, a carbonated OCP is unlikely to exist [28], the presence of a carbonated phase could indicate the presence of another calcium phosphate phase. According to the XRD data, this could be a poorly crystalline apatite phase in addition to the main OCP phase. Labile non-apatitic environments were detected on the basis of bands corresponding to labile HPO_4 groups in the υ_4 PO_4 domain and labile carbonate. The presence of a labile environment on the HA/amTCP *Top Powder*, known to belong to a hydrated layer on the surface of crystals, was confirmed by the band decomposition performed on the 700–450 cm^{-1} domain (Fig. 6c), which showed the presence of labile non-apatitic PO_4^{3-} (617 cm^{-1}) and HPO_4^{3-} (530 cm^{-1}) species, thus confirming the hypothesis of the existence of a hydrated layer [2].

Regarding the HA/amTCP blend, OCP and a poorly crystallized, carbonated apatite were observed in the final *Top Powder*. In order to determine the distribution of phases in the complex plate-like structure of this powder, Raman micro-spectroscopy was performed.

Raman spectroscopy

A part of the main plate composing the *Top Powder* was collected. This portion allowed the side of the main plate to be observed and went 200 μm deep in the direction of the centre of the main plate. The analysis of this volume provided information on the composition of the entire volume of the newly precipitated phase. A 3D analysis was carried out (Fig. 8), and the mapping was performed on the entire volume. Here, three z levels are presented, corresponding to the plate-like surface (z = 0 μm), the core of the plate (z = 5 μm) and the flat surface (z = 10 μm).

First, two extreme spectra, taken on the flat (z = 10 μm) and platelet-like (z = 0 μm) surfaces of the plate, are presented in Fig. 7. Spectral decomposition was performed on the 1100–850 cm^{-1} spectral domain in order to identify the participation of each calcium phosphate composing the plate (OCP or apatite). This type of analysis differentiated between these two calcium phosphates thanks several clear differences in their spectra. On a large scale of any spectrum composed of OCP and apatite, the first differences can be observed in the υ_3 PO_4 band area. In this domain, the OCP phase shows two bands, at 1011 and 1005 cm^{-1}. Another difference can be noticed at 916 cm^{-1}, where OCP presents a band corresponding to the P–(OH) stretch of HPO_4 [6], while apatite shows no band. The difference between these two calcium phosphates is also visible on the main υ_1 PO_4 characteristic domain. The apatite phase presents only one band at 960 cm^{-1}, whereas the OCP phase has two bands, at 966 and 959 cm^{-1}. Therefore, an enlargement of the band around 960 cm^{-1} can be seen when OCP is present.

Spectrum decomposition: from sheet-like side to surface of the HA/amTCP Top Powder

According to the decomposition of this Raman band (1100–850 cm^{-1}) of the flat surface in contact with the atmosphere (z = 10 μm), which was in contact with the air after CO_2 treatment, the powder appears to be mainly composed of an apatite phase close to HA [characteristic peaks: 961 cm^{-1} (υ_1 PO_4), 1077–1029 cm^{-1} (υ_3 PO_4)] [4] and a small amount of OCP phase [characteristic bands: 966, 959 cm^{-1} (υ_1 PO_4), 1112–1005 cm^{-1} (υ_3 PO_4)], as shown in Fig. 8. The υ_1 PO_4 band is narrow and mostly composed of the 961 cm^{-1} band, which, as noted previously, is characteristic of the apatite phase.

In contrast, on the decomposition of the spectrum obtained on the sheet-like surface, a greater contribution of OCP phase can be observed, visible with the 966 and 958 cm^{-1} bands, compared to the apatite phase at 961 cm^{-1}. The OCP phosphate band at 1007 cm^{-1} (υ_3 PO_4) is also more intense on the plate-like surface (z = 0 μm) than on the flat one (z = 10 μm) of the HA/amTCP *Top Powder*. This indicates a higher proportion of OCP phase and is in agreement with the platelet-like crystals observed by SEM (Fig. 9, HA/amTCP *Top Powder*). On the plate-like surface (z = 0 μm), the spectrum corresponds to almost pure OCP, with a small peak at 948 cm^{-1}, indicating the presence of a small amount of an amorphous phase.

The difference in composition is clear when the measurements corresponding to each side of the sample (at z = 0 and 10 μm) are compared. In both cases, the υ_1 PO_4 band always corresponds to apatite (962 cm^{-1}) and OCP (966 and 958 cm^{-1}) phases. The relative importance of the two species was evaluated (Fig. 8) by calculating the ratio between the area of

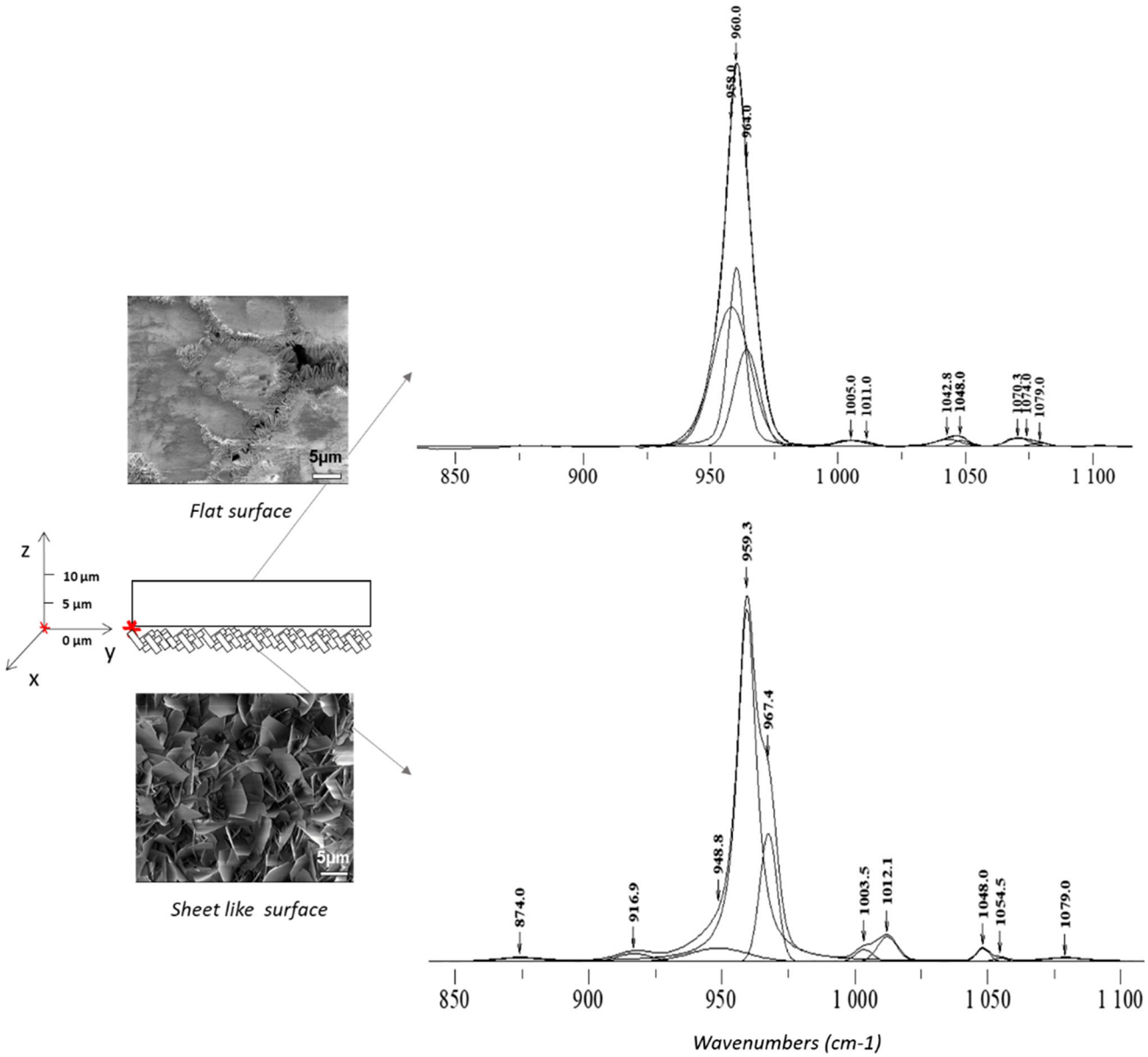

Figure 7 Raman spectrum of HA/amTCP Top Powder at z = 0 µm, which is the plate-like surface (mostly in contact with the solution) and at z = 10 µm, the flat surface (mostly in contact with air).

the υ_3 PO_4 band of OCP (1015–990 cm^{-1}) phase and the total area of the υ_1 PO_4 band, which corresponds to the contribution of all the calcium phosphate phases (980–940 cm^{-1}) present in the sample. At z = 10 µm, apatite is observed to be predominant (r = 0.04). This ratio shows a similar predominance of the apatite phase at z = 5 µm (r = 0.04) (Fig. 8a), while, at z = 0 µm, OCP appears as the main phase (r = 0.08).

Multidimensional analysis of HA/amTCP Top Powder

To go further in the analysis of the composition of the HA/amTCP *Top Powder* plate, all the spectra taken in the 3D volume were analysed. The area ratio discussed previously was calculated on each sample, and the results are presented in Fig. 8. The difference of ratio between the two phases of calcium phosphate that are present (OCP and apatite phases) is highlighted by the colour scale. The plot of the band area ratio [area of the υ_3 PO_4 band of OCP (1015–990 cm^{-1})

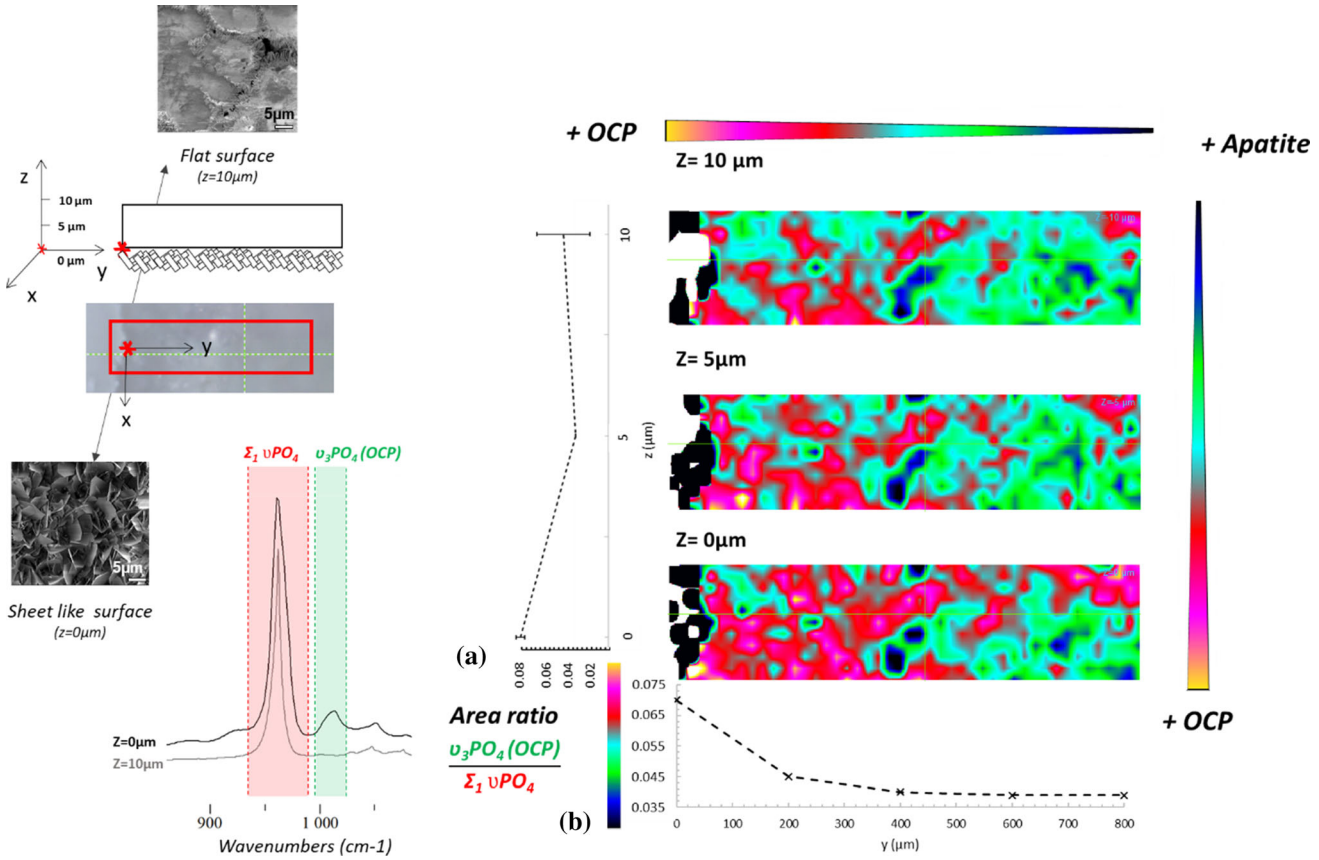

Figure 8 3D Raman cartography of HA/amTCP Top Powder with the υ_1 PO_4(OCP)/Σ $\upsilon 1$ PO_4 band area ratio at z = 0, 5 and 10 µm.

Figure 9 SEM micrographs of HA/amTCP Top Powder, **a** at z = 10 µm, **b** at z = 0 µm.

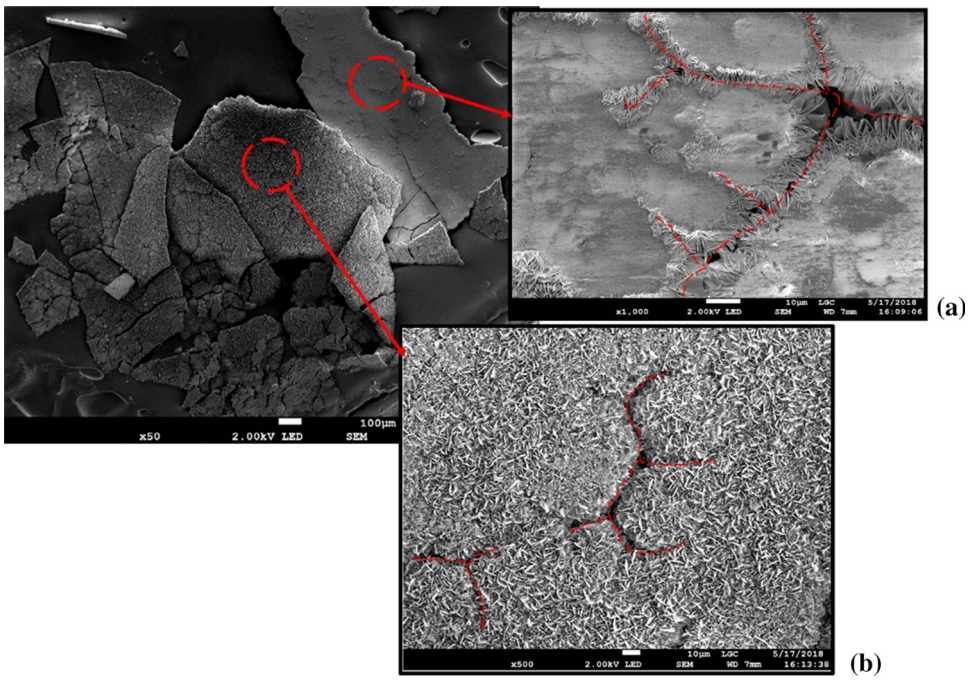

divided by the total area of the υ_1 PO_4 band (980–940 cm^{-1}) from the centre to the edge of the plate (Fig. 8b] shows a nonlinear gradient of composition, going from the centre, where a high proportion of apatite (blue/green) is present, to the edge, where the proportion of OCP (yellow/pink) is higher.

The three selected "slices" of the 3D analysis of HA/amTCP *Top Powder* shown in Fig. 8 confirm the presence of OCP phase, mainly on the edge and on the sheet-like surface (solution side during CO_2 treatment). In addition to a different ratio of OCP/phosphate phases on the *y* and *z* axes allowing a large-scale analysis (from the side of the plate to 200 μm further towards the centre), this 3D view also allows a gradient of composition to be observed at a smaller scale. This observation can be related to the SEM micrographs (Fig. 9), where the large plate seems to be composed of smaller ones that have merged together through entanglement of platelet crystals mainly observable on the surface of each plate (Fig. 9a).

Figure 9 shows a part of the main plate on both sides (flat and plate-like surfaces) where some cracks are visible. These cracks could correspond to the merging lines between the original smaller plates observed on the SEM pictures.

Discussion

Calcium phosphate precipitation in aqueous media has been thoroughly investigated in numerous studies, which shows that pH and temperature [2, 9], along with supersaturation/concentration, are key parameters controlling the nature of the calcium phosphate phases formed. In the present work, a high-pressure CO_2 treatment at fixed temperature and pressure (40 °C, 80 bar) was implemented to modify HA, amTCP and HA/amTCP ceramic powders. From analyses of powders after this treatment, a general description can be given of the phenomena involved, despite some noticeable differences identified between the three ceramic powders. It is important to stress that, in this study, due to experimental difficulties related to high-pressure conditions, it was not possible to measure the pH or the concentrations of species in situ during the CO_2 treatment. Therefore, at this stage, it is only possible to propose hypotheses based on the characterization of the final powders.

As described in the Materials and methods section, the aqueous environment in which modification of the ceramics takes place undergoes several pH changes during the course of the process. The first change occurs early in the process, during the step of CO_2 dissolution in the water in which the powders have been placed (Fig. 2). During this step, the pH of the water drops from neutral to 3.2, which corresponds to the pH of CO_2-saturated water at 37 °C [21]. At such a pH, the ceramic powders start to dissolve, thus releasing the ionic species composing them into the aqueous medium. The aqueous environment at the ceramic surface contains many ionic species, especially H_3O^+, OH^-, CO_3^{2-}, Ca^{2+}, HPO_4^{2-}, HCO_3^- and PO_4^{3-}. Apart from the carbonates, all of them come from the partial dissolution of the solid phase and, therefore, occur through a protonation mechanism. The electrical neutrality of the environment is ensured. This partial dissolution also leads to a local increase in pH related to the release of phosphate ions and OH^-.

During the degassing step, the progressive release of the dissolved CO_2 leads to an increase in the pH value, starting from the surface of the liquid (top surface, Fig. 2) and spreading to the bulk. After 1 h, the pH of the solution is completely neutralized (pH 7). At the same time, during this step of the process, some of the water evaporates while CO_2 is released, which induces a rapid increase in the ionic concentrations, which can reach the nucleation threshold [29], depending on the local pH, and can lead to the precipitation of calcium phosphate species.

In the case of HA/amTCP and HA experiments, this partial dissolution of powders associated with a pH increase from acidic to neutral pH could lead to the formation of OCP phase. This is a stable calcium phosphate phase from moderately acidic up to neutral pH values. Its presence in the *Top Powder* at the end of the process is consistent with this hypothesis. At low supersaturation, a polynuclear nucleation and crystal growth process corresponding to OCP formation could be involved, as shown by Heughebaert et al. [30]. This hypothesis is confirmed by the observation of this new phase on the surface. Then, OCP crystallization is assumed to proceed in the radial direction from the grain surface, until several small plates come into contact to form a bigger one

(Fig. 9), eventually leading to an entirely covered surface.

An evolution in the z direction, which corresponds to the depth of the plate, is also observable. The ceramic therefore also evolves, growing from the surface (air–solution interface) to the bottom of the container, where the pH is slightly lower due to the remaining dissolved CO_2. This promotes the formation of OCP phase and also other calcium phosphate phases. Slight presence of an amorphous phase and an apatite phase has been detected [9].

The Raman spectroscopy analysis of the HA/amTCP *Top Powder* at $z = 0$ µm shows a slight presence of an amorphous calcium phosphate. It is important to note that this additional phase is not present at $z = 10$ µm, where calcium phosphate is more mature and has already transformed into apatite phase. This amorphous phase could be the remaining part of the initial calcium phosphate phase formed at the beginning of the precipitation step; amorphous calcium phosphate is the least stable calcium phosphate phase involved and should thus nucleate first.

In the case of HA/amTCP *Top powder*, it has also been shown that the proportion of apatite phase seems to be higher at the centre of the plate and on its top, where the ceramic is closer to the surface of the liquid and the pH is slightly less acidic during the depressurization step. This could be due to a gradual conversion of OCP into apatite phase. This phenomenon of hydrolysis of OCP into apatite has been widely investigated in the literature and shown to occur at different rates depending on the temperature and pH [30, 31]. However, given that the phosphate concentration evolves constantly, it is difficult to evaluate the conversion rate. It is well known that non-stoichiometric apatites can be obtained by precipitation of a thermodynamically non-stable phase, such as DCPD or OCP, which can evolve according to the Ostwald rule [31, 32]. The conversion of OCP into apatite is based on a reorganization of the lattice into a hexagonal structure with a partial loss of water, phosphate ionic species and probably calcium [33]. Because this phenomenon tends to totally convert OCP into apatite over time, it can be referred to as a maturation process. This is known to be enhanced in the presence of HCO_3^-, which is the case here during the degassing phase [22, 34]. However, the presence of CO_3^{2-} is also known to be an inhibitor of this conversion [2]. Unfortunately, due to the experimental conditions, the kinetics of precipitation and conversion was difficult to apprehend.

The Raman cartography allowed us to observe that OCP seemed to undergo this maturation phenomenon at the same time as fusion of the final plate took place. The conversion of OCP into apatite could also happen during the formation of the bigger plate, provided that ionic diffusion can occur. This could be related to a poly-maturation phenomenon. The ratio of the υ_3 OCP/υ_1 PO_4 of the total phosphate phases highlights a nonlinear composition and thus an evolution of the OCP phase into apatite phase along the z or y axis. The conversion occurs in every direction as nucleation and crystal growth continues. Because the edge of the plate is still rich in OCP and considering previous results [30], it can be hypothesized that the OCP phase growth is faster than its conversion to apatite phase.

It is also important to note that such a growth of calcium phosphate causes the concentration of the solution to evolve continuously, because of OCP precipitation on the one hand and because of conversion to apatite, leading to calcium concentration decreases and/or release of some phosphate ions [35], on the other. This conversion could also lead to a slight change of pH [35].

Thanks to the FTIR spectroscopy data, the presence of non-apatitic carbonate groups associated with a hydrated layer on biomimetic apatite nanocrystals has been confirmed in the case of treated HA and HA/amTCP *Top Powders*. This hydrated layer is also confirmed by the decomposition of the FTIR spectrum of the *Top Powder* of HA/amTCP, which shows some non-apatitic PO_4^{3-} (617 cm^{-1}) and HPO_4^{2-} (530 cm^{-1}) ionic environments.

The observation and hypothesis made for *Top Powder* of the HA/amTCP are likely to be extended to the HA *Top Powder* because of their similarity in morphology and also their similar chemical composition and structure. The main difference lies in the size of the plate-like structure on the one side of the plate of the *Top Powders* (Fig. 7g). The one on HA/amTCP is larger, possibly because of the higher solubility of amTCP in the aqueous medium, which leads to the release of a greater amount of calcium, available for OCP phase growth.

According to XRD and FTIR spectroscopic analyses, the *Bottom Powder* samples of HA and HA/amTCP are very similar in composition. It is interesting to note that amTCP present in the HA/amTCP

(Fig. 7q) blend seems to be totally converted at the end of the experiment, confirming the hypothesis that this phase is preferentially dissolved in such conditions.

However, even though the amTCP experiment has shown some similarities with experiments on pure HA and HA/amTCP, such as the carbonate content as evaluated by FTIR spectroscopy or the presence of OCP and apatite phases in the *Top Powder*, a different morphology has also been shown and, interestingly, the presence of DCPD has been evidenced. During the CO_2 dissolution step of the process, the amTCP phase, which is more soluble in water than HA is under these conditions [9], can be expected to dissolve preferentially. In the specific case of pure amTCP, the solid dissolution phenomenon leads to a large release of ionic species into the aqueous medium. These species are able to reach the nucleation threshold at the bottom of the container before the degassing phase, while CO_2 is still dissolved in the water (low pH). In that case, the calcium phosphate phase initially formed could correspond to a DCPD phase, the precipitation of which is favoured in moderately acidic media (pH around 5) [9]. This DCPD phase could then be very easily hydrolysed into OCP [9] at a pH of 5–6.8, a pH range reached during the degassing step. This hydrolysis would rely on a dissolution/precipitation phenomenon [2] following the Ostwald rule [31], supporting the concept that the first precipitated phase is not necessarily the most thermodynamically stable. This hypothesis has been confirmed by the presence of a DCPD phase, as observed on the XRD patterns of the treated amTCP *Bottom Powder* and *Top Powder* (Fig. 3b).

The *Bottom* and *Top Powder*s of the amTCP experiment present very specific morphologies in comparison with HA and HA-/amTCP-treated samples. They are both composed of spheres, smooth or "flower-like" structures. It is nonetheless important to note a plate arrangement in the case of the *Top powder*, which is similar to that of the other *Top Powder* samples. Spheres of this kind have already been observed using a CO_2 bubble templating process [27, 28]. However, this process uses different chelating ions (EDTA or citric acid) in order to form small spherical CO_2 bubbles in the aqueous environment, which is different from the strategy used in the present study. Nonetheless, the structures that have been observed are very similar. In the present work, the CO_2 bubbles can act as nucleation sites by locally modifying the surface tension, concentration and also the pH. If enough calcium phosphate is dissolved in the first stage of the process, as is the case with amTCP-treated powder, the supersaturation level is likely to be reached, leading to crystallization.

The morphologies of solid structures observed by SEM can be explained according to different studies that have shown the formation of similar apatite spheres. The size of the platelets that are observed to cover the surface of some of the spheres could depend on various parameters such as pressure or pH [27, 36]. This covering mechanism is favoured by a slightly acidic pH [36]. Therefore, in the amTCP experiment, a local change of pH, likely to occur because of the conversion of OCP to apatite phase [9], could be the driving force for the growth of sheets.

Conclusion

We have shown that the use of an innovative high-pressure CO_2 process makes it possible to transform commonly used calcium phosphate, i.e. HA, amTCP and HA/amTCP blend, from both the chemical and microstructural points of view, in the aim of obtaining biomimetic apatite. A dissolution of the initial powder has been observed and depends on its nature, the amTCP being much more soluble. The new phase obtained was also dependent on the initial calcium phosphate that was used. With amTCP, DCPD was only observed in a very low proportion. The main phase observed in each sample was OCP, which has been shown to undergo a maturation process and lead to the formation of a PCCA. Thus, these modified ceramics should present physical and chemical properties close to those of the mineral phase of bone and could have a great potential in bone regeneration.

This hydrothermal, low-temperature method could therefore be used to modify existing bioceramics, such as the commonly used porous biphasic calcium phosphate ceramics, to create a new biomimetic calcium phosphate coating that could increase their reactivity and bioactivity and promote bone neoformation.

Acknowledgements

We thank the Federal University of Toulouse and the Région Occitanie (France) for the PhD grant of Clémentine Aubry. We are also grateful to the Teknimed Company for providing HA powder.

References

[1] LeGeros RZ (1981) Apatites in biological systems. Prog Cryst Growth Charact 4:1–45

[2] Drouet C, Grossin D, Sarda S, Cazalbou S, Rey C (2018) Apatites biomimétiques Des biominéraux aux analogues de synthèse pour le biomédical. Techniques de l'ingénieur Biomatériaux biomécanique 33(IN227):V1

[3] Weiner S, Wagner HD (1998) The material bone: structure–mechanical function relations. Annu Rev Mater Sci 28:271–298

[4] Rey C, Marsan O, Combes C, Drouet C, Grossin D, Sarda S (2014) Characterization of calcium phosphates using vibrational spectroscopies. In: Ben-Nissan B (ed) Advances in calcium phosphate biomaterials. Springer series in biomaterials science and engineering, vol 2. Springer, Berlin, pp 229–266

[5] Cazalbou S, Eichert D, Drouet C, Combes C, Rey C (2004) Minéralisations biologiques à base de phosphate de calcium. C R Palevol 3:563–572

[6] Rey C, Shimizu M, Collins B, Glimcher MJ (1990) Resolution-enhanced Fourier transform infrared spectroscopy study of the environment of phosphate ions in the early deposits of a solid phase of calcium-phosphate in bone and enamel, and their evolution with age. I: investigations in the v_4PO_4 domain. Calcif Tissue Int 46:384–394

[7] Kokubo T (1991) Bioactive glass ceramics: properties and applications. Biomaterials 12:155–163

[8] S. Cazalbou (2000) Échanges cationiques impliquant des apatites nanocristallines analogues au minéral osseux. PhD dissertation, University of Toulouse

[9] Elliott JC (1994) Structure and chemistry of the apatites and other calcium orthophosphates, vol 18. Elsevier Science, Amsterdam

[10] Haute Autorité de Santé Substituts osseux Saint-Denis La Plaine : HAS, 2013: 134

[11] Tian J, Tian J (2001) Preparation of porous hydroxyapatite. J Mater Sci 36:3061–3066. https://doi.org/10.1023/A:1017935411108

[12] Autefage H (2009) Rôle ostéoinducteur d'un revêtement d'apatite carbonatée nanocristalline sur des céramiques de phosphate de calcium biphasique. PhD dissertation, University of Toulouse

[13] Aroso IM, Craveiro R, Rocha A, Dionisio M, Reis RL, Paiva A, Duarte AR (2015) Design of controlled release systems for THEDES—therapeutic deep eutectic solvents, using supercritical fluid technology. Int J Pharm 492:73–79

[14] Martins M, Baros A, Quraishi S, Gurikov P, Raman SP, Smirnova I, Duarte ARC (2015) Preparation of macroporous alginate-based aerogels for biomedical applications. J Supercrit Fluids 106:152–159

[15] Duarte ARC, Caridade SG, Mano JF, Reis RL (2009) Processing of novel bioactive polymeric matrixes for tissue engineering using supercritical fluid technology. Mater Sci Eng C 29:2110–2115

[16] Wakayama H (2018) $CaCO_3$–polymer nanocomposite prepared with supercritical CO_2. Int J Polym Sci. https://doi.org/10.1155/2018/9783941

[17] Duarte ARC, Santo VE, Gomes ME, Reis RL (2018) Supercritical fluid technology as a tool to prepare gradient multifunctional architectures towards regeneration of osteochondral injuries. Adv Exp Med Biol 1058:265–278

[18] Li W, Yu Q, Wu P (2009) Submicronic calcite particles with controlled morphology tailored by polymer skeletons via carbonation route with compressed or supercritical CO_2. Green Chem 11:1541–1549

[19] Matsuya S, Lin X, Udoh KI, Nakagawa M, Shimogoryo R, Terada Y, Ishikawa K (2007) Fabrication of porous low crystalline calcite block by carbonation of calcium hydroxide compact. J Mater Sci Mater Med 18:1361–1367

[20] Teir S (2008) Fixation of carbon dioxide by producing carbonates from minerals and steel making slags. PhD dissertation, University of Helsinki

[21] Peng GMC, Crawshaw JP (2013) The pH of CO_2-saturated water at temperatures between 308 and 423 K at pressures up to 15 MPa. J Supercrit Fluids 82:129–137

[22] Barrere F, Van Blitterswijk CA, De Groot K, Layrolle P (2002) Influence of ionic strength and carbonate on the Ca-P coating formation from SBF× 5 solution. Biomaterials 23:1921–1930

[23] Heughebaert JC (1977) Contribution à l'étude de l'évolution des orthophosphates de calcium précipités amorphes en orthophosphates apatitiques, Doctoral dissertation, University of Toulouse

[24] Vandecandelaere N, Rey C, Drouet C (2012) Biomimetic apatite-based biomaterials: on the critical impact of synthesis and post-synthesis parameters. J Mater Sci Mater Med 2:2593–2606

[25] Rey C, Renugopalakrishman V, Collins B, Glimcher MJ (1991) Fourier transform infrared spectroscopic study of the

carbonate ions in bone mineral during aging. Calcif Tissue Int 49:251–258

[26] Lin K, Wu C, Chang J (2014) Advances in synthesis of calcium phosphate crystals with controlled size and shape. Acta Biomater 10:4071–4102

[27] Cheng X, He Q, Li J, Huang Z, Chi RA (2009) Control of pore size of the bubble-template porous carbonated hydroxyapatite microsphere by adjustable pressure. Cryst Growth Des 9:2770–2775

[28] Cheng X, Huang Z, Li J, Liu Y, Chen C, Chi R (2010) Self-assembled growth and pore size control of the bubble-template porous carbonated hydroxyapatite microsphere. Cryst Growth Des 10:1180–1188

[29] Duan YR, Zhang ZR, Wang CY, Chen JY, Zhang XD (2005) Dynamic study of calcium phosphate formation on porous HA/TCP ceramics. J Mater Sci Mater Med 16:795–801

[30] Heughebaert JC, Nancollas GH (1984) Kinetics of crystallization of octacalcium phosphate. J Phys Chem 88:2478–2481

[31] Natsuko I, Masanobu K, Setsuaki M, Noriaki W, Koji O (2010) Hydrothermal synthesis and characterization of hydroxyapatite from octacalcium phosphate. J Ceram Soc Jpn 118:762–766

[32] Nývlt J (1995) The Ostwald rule of stages. Cryst Res Technol 30:443–449

[33] Brown WE (1962) Crystallographic and chemical relations between octacalcium phosphate and hydroxyapatite. Nature 196:1050–1055

[34] Cheng P (1987) Formation of octacalcium phosphate and subsequent transformation to hydroxyapatite at low supersaturation: a model for cartilage calcification. Calcif Tissue Int 40:339–343

[35] Eliaz N, Eliyahu M (2007) Electrochemical processes of nucleation and growth of hydroxyapatite on titanium supported by real-time electrochemical atomic force microscopy. J Biomed Mater Res, Part A 80:621–634

[36] He QJ, Huang ZL (2007) Controlled growth and kinetics of porous hydroxyapatite spheres by a template-directed method. J Cryst Growth 300:460–466